Наносистеми, наноматеріали, нанотехнології
Nanosystems, Nanomaterials, Nanotechnologies
2012, т. 10, № 4, сс. 897–916

PACS numbers: 61.50.Ah, 61.72.Bb, 64.60.De, 64.60.qe, 64.75.Jk, 75.30.Hx, 81.30.-t

Modelling of Physical Kinetics of Relaxation in Macroscopically Homogeneous F.C.C.-Ni–Fe Alloys

I. V. Vernyhora[1,2], S. M. Bokoch[3,4], and V. A. Tatarenko[1]

[1]*G. V. Kurdyumov Institute for Metal Physics, N.A.S. of Ukraine,*
Department of Solid State Theory,
36 Academician Vernadsky Blvd.,
UA-03680 Kyyiv-142, Ukraine
[2]*Institute for Applied Physics, N.A.S. of Ukraine,*
Department of Modelling of Radiation Effects
and Microstructure Transformations in Construction Materials,
58 Petropavlivska Str.,
UA-40030 Sumy, Ukraine
[3]*Institute for Advanced Materials Science and Innovative Technologies,*
Department of Materials Design and Technology,
15 Sauletekio Ave.,
LT-10224 Vilnius, Lithuania
[4]*NIK Electronics,*
34 Lesi Ukrayinky Blvd.,
UA-01601 Kyyiv, Ukraine

In comparison with classical Lifshitz–Slyozov–Wagner's theory and, where it is possible, with available experimental data, the physical kinetics of evolution of a microstructure of f.c.c.-Ni–Fe alloys is simulated by means of the Onsager-type equations of microdiffusion and with the account of the effects caused by magnetic interatomic interactions and elastic interactions of inclusions of phases. Magnetism proper in f.c.c.-Ni–Fe alloys essentially influences a tendency to atomic ordering and development of their microstructure; magnetic interactions promote stabilisation of a precipitated phase and dilate an interval of two-phase coexistence. In Elinvar alloys, elastic interactions essentially change morphology of an intermixture of formed phases of the superstructural $L1_0$ and $L1_2$ types (or of structural $A1$ type), giving the anisotropic character to the shape of inclusions of phases as well as to their relative spatial arrangement. Meanwhile, for an intermixture of phases of structural $A1$ type and superstructural $L1_2$ type in Permalloys, the anisotropic effects of such interactions are inappreciable.

У порівнянні з класичною теорією Ліфшиця–Сльозова–Ваґнера і, де можливо, з наявними експериментальними даними змодельовано фізичну

кінетику еволюції мікроструктури стопів ГЦК-Ni–Fe за допомогою рівнань мікродифузії Онсаґерового типу та з урахуванням ефектів, спричинених магнетними міжатомовими взаємодіями та пружніми взаємодіями вкраплень фаз. Властивий стопам ГЦК-Ni–Fe магнетизм істотно впливає на тенденцію до атомового впорядкування та розвиток їхньої мікроструктури: магнетні взаємодії сприяють стабілізації фази, що виділяється, та розширюють інтервал співіснування фаз парами. Пружні ж взаємодії істотно змінюють морфологію суміші утворених фаз надструктурного типу $L1_0$ і $L1_2$ (або структурного типу $A1$) в елінварних стопах, надаючи анізотропного характеру як формі вкраплень фаз, так і їхньому взаємному розташуванню; але для суміші фаз структурного типу $A1$ та надструктурного типу $L1_2$ в пермалоях анізотропні ефекти таких взаємодій є незначними.

В сравнении с классической теорией Лифшица–Слёзова–Вагнера и, где возможно, с имеющимися экспериментальными данными смоделирована физическая кинетика эволюции микроструктуры сплавов ГЦК-Ni–Fe с помощью уравнений микродиффузии онсагеровского типа и с учётом эффектов, вызванных магнитными межатомными взаимодействиями и упругими взаимодействиями включений фаз. Присущий сплавам ГЦК-Ni–Fe магнетизм существенным образом влияет на тенденцию к атомному упорядочению и развитие их микроструктуры: магнитные взаимодействия способствуют стабилизации фазы, которая выделяется, и расширяют интервал попарного сосуществования фаз. Упругие же взаимодействия существенным образом изменяют морфологию смеси образованных фаз сверхструктурного типа $L1_0$ и $L1_2$ (или структурного типа $A1$) в элинварных сплавах, придавая анизотропный характер, как форме включений фаз, так и их взаимному расположению, но для смеси фаз структурного типа $A1$ и сверхструктурного типа $L1_2$ в пермаллоях анизотропные эффекты таких взаимодействий являются незначительными.

Key words: Ni–Fe alloys, phase transformation, physical kinetics, coarsening.

(Received 19 September, 2012)

1. INTRODUCTION

Ni–Fe alloys are well known as widely used materials in up-to-date industrial and technological applications due to their inimitable physical properties (low thermal expansion, unique elastic properties, high permeability, and low coercive force), the majority of which is formed due to the coexistence and significant mutual influence of magnetic and spatial atomic orders. From the experimentally observed phase diagram (that is 'metastable' in fact; Fig. 1), one can notice that the temperature decrease leads to the following sequential phase transformations: the 2^{nd}-order paramagnetic–ferromagnetic phase transition and the 1^{st}-order (dis)order–order phase transformations. Depending on the Fe (Ni) concentration (c_{Fe} (c_{Ni})) and the external conditions (temperature (T), pressure (p), magnetic field (**B**), *etc.*), the latter results in

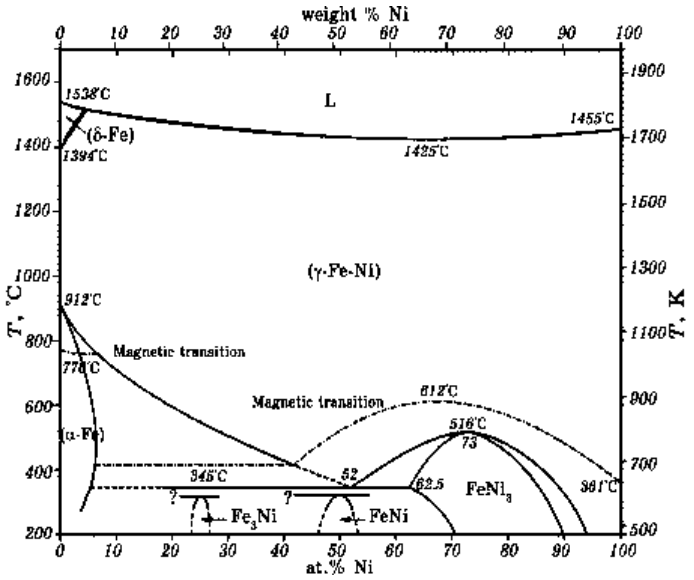

Fig. 1. Experimentally obtained 'metastable' phase diagram of Ni–Fe alloys (according to Ref. [2]). The symbol '?' denotes the unidentified authentically structural and/or magnetic states of the alloys at issue. γ-Fe, α-Fe and δ-Fe are the f.c.c., low- and high-temperature b.c.c. lattice-based modifications of an iron. L is the Ni–Fe liquid solution. The equilibrium crystal structures of the three stoichiometric ordered phases at $T = 0$ K, $L1_2$-Ni_3Fe (Permalloy), $L1_0$-NiFe (Elinvar) and $L1_2$-$NiFe_3$ (Invar), are also shown (right-to-left).

the formation of the ordered alloys with substitutional f.c.c. $L1_2$-type (super)structures (which are experimentally observed for Ni_3Fe stoichiometry and theoretically proposed for $NiFe_3$) or f.c.c. $L1_0$-type ones (*e.g.*, for NiFe) from the disordered solid solutions of f.c.c.-$A1$ type (characterized by the short-range atomic order only) [1, 2]. The interplay between the magnetic and structural orders becomes apparent when studying the ordering processes in these alloys. Notably, the magnetic nature of the alloy components promotes the atomic ordering and the formation of the ordered (super)structures mentioned above. Moreover, in the magnetic state of an alloy, the (Kurnakov) ordering temperatures, $T_K(c_{Fe})$, are enhanced (for example, see Refs. [3–6]). In turn, as was shown previously [5–8], the Curie temperature, $T_C(c_{Fe})$, of the ordered alloys also increases, comparing to the disordered ones (including the alloys with a short-range atomic order), *e.g.*, for NiFe-type Elinvar and Ni_3Fe-type Permalloy alloys, the excess is about 100–200 K and 100 K, respectively. Therefore, the theoretical investigation of magnetic and atomic order effects in these alloys becomes an important part of deeper understanding a variety of physical phenomena.

In spite of number of works (see, *e.g.*, Refs. [9, 10] and references

therein) devoted to the study of the thermodynamic behaviour of f.c.c.-Ni–Fe alloys, only a few of them address the investigation of the order–disorder phase transformation kinetics. For example, in [11], the authors studied all stages (nucleation, growth, and further coarsening) inherent to the 1st-order transformation in Ni_3Fe Permalloy alloy by means of experimental measurements (SEM technique and x-ray diffraction). They showed that the degree of order in these alloys is sensitive to the annealing temperature and decreases with temperature increasing; the ordering kinetics, notably, the domain structure and the impurity effects, was investigated too. Nevertheless, the role of magnetism was analysed neither experimentally nor theoretically. It is also necessary to mention the lack of kinetics investigation for NiFe Elinvar, where, besides the magnetic effects, the elastic effects can perform the crucial role in the microstructure formation. Due to the slowness of the diffusion processes, the experimental observation of ordered structures in these alloys is rather difficult and, thus, the theoretical modelling becomes a useful tool in the investigation of the ordering processes.

In a given work, we study the effects of magnetism and elasticity (induced by the size mismatch between the constituent atoms) on the formation of the ordered structures in Permalloy and Elinvar alloys. In Section 2, we formulate a model used to calculate the kinetics of order–disorder transformation. The obtained results are presented and discussed in Sec. 3 and are followed by the overall conclusion in Sec. 4.

2. MODEL

On the microscopic level, the physical kinetics of phase transformations can be described, using the Onsager-type microscopic diffusion equations. Within the scope of the concentration waves (and in particular, the static concentration waves—SCW) representation, such an approach was firstly proposed by Khachaturyan [12, 13]. The morphology of a two-phase alloy is described by a single-site probability function, $p(\mathbf{r},t)$, which is the probability of finding a solute atom β (*e.g.*, Fe in Ni_3Fe and NiFe alloys) at a lattice site $\mathbf{r}$ and at an instant time t. The diffusional relaxation of a binary α–β alloy is described by the equation [12, 13]:

$$\frac{dp(\mathbf{r},t)}{dt} \approx \frac{c_\beta(1-c_\beta)}{k_B T} \sum_{\mathbf{r}'} L(\mathbf{r}-\mathbf{r}') \frac{\delta \Delta F}{\delta p(\mathbf{r}',t)}, \qquad (1)$$

where c_β is the atomic fraction of solute (β) atoms, k_B is the Boltzmann constant, T is the absolute temperature; $L(\mathbf{r}-\mathbf{r}')$ is the Onsager kinetic coefficients related to the substitutional atoms' mobilities by means of appropriate diffusion mechanism between the sites $\mathbf{r}$ and $\mathbf{r}'$; ΔF is the configuration-dependent part of the total Helmholtz free energy (per site) including three contributions: 'electrochemical', magnetic and

elastic ones, *i.e.* $\Delta F = \Delta F_{\text{chem}} + \Delta F_{\text{magn}} + \Delta E_{\text{elast}}$. The sum is carried out over all N sites of the Bravais lattice. The kinetic equation (1) approximates the evolution rate by the first non-vanishing term of its expansion with respect to the thermodynamic driving force, $\delta\Delta F/\delta p(\mathbf{r},t)$ (small driving force). Within the long-wave approximation, Eq. (1) transforms into the conventional Cahn–Hilliard equation [14].

Within the scope of the self-consistent-field approximation, the configuration-dependent part of free energy of binary substitutional alloys is defined as follows [12, 13]:

$$\Delta F \cong \frac{1}{2N}\sum_{\mathbf{k}\in BZ}\tilde{w}(\mathbf{k})\left|\tilde{p}(\mathbf{k})\right|^2 + k_B T\sum_{\mathbf{r}}\{p(\mathbf{r})\ln p(\mathbf{r}) + [1-p(\mathbf{r})]\ln[1-p(\mathbf{r})]\} - \\ -T\Delta S_{\text{magn}}; \qquad (2)$$

here, $\tilde{w}(\mathbf{k}) = \Sigma_{\mathbf{r}} w(\mathbf{r})\exp(-i\mathbf{k}\cdot\mathbf{r})$ is the Fourier transform of total 'mixing' energies, $\{w(\mathbf{r})\}$, and $\tilde{p}(\mathbf{k}) = \Sigma_{\mathbf{r}} p(\mathbf{r})\exp(-i\mathbf{k}\cdot\mathbf{r})$ is the Fourier transform of probability function, $p(\mathbf{r})$. The summation over $\mathbf{r}$ is carried out over all the Bravais lattice sites; the summation over $\mathbf{k}$ is over all points of quasi-continuum within the 1st Brillouin zone (BZ) of such lattice permitted by the periodic boundary conditions. Assuming the interatomic interactions within the four coordination shells of f.c.c. lattice, $\tilde{w}(\mathbf{k})$ is defined as

$$\tilde{w}(\mathbf{k}) \cong 4w_1(\cos\pi h\cos\pi k + \cos\pi h\cos\pi l + \cos\pi k\cos\pi l) + \\ +2w_2(\cos 2\pi h + \cos 2\pi l + \cos 2\pi k) + \\ +8w_3(\cos 2\pi h\cos\pi k\cos\pi l + \cos 2\pi k\cos\pi h\cos\pi l + \cos 2\pi l\cos\pi h\cos\pi k) + \\ + 4w_4(\cos 2\pi h\cos 2\pi k + \cos 2\pi h\cos 2\pi l + \cos 2\pi k\cos 2\pi l) + \ldots; \qquad (3)$$

here, w_1, w_2, w_3, w_4, ... are the values of the effective interchange ('mixing') energies of substitutional atoms, $w(\mathbf{r}) = w_{\text{prm}}(\mathbf{r}) + w_{\text{magn}}(\mathbf{r}) = (w_{\text{chem}}(\mathbf{r}) + V_{\text{si}}^{\beta\beta}(\mathbf{r})) + w_{\text{magn}}(\mathbf{r})$, for the 1st, 2nd, 3rd, 4th, ... neighbouring coordination shell, respectively; $V_{\text{si}}^{\beta\beta}(\mathbf{r})$ is the strain-induced contribution (due to the atomic-size mismatch) in the 'mixing' energy; (h,k,l) are continuous dimensionless coordinates of the wave vector defined as $\mathbf{k} = (k_x,k_y,k_z) = (2\pi/a)(h,k,l)$ (a is the equilibrium lattice parameter of f.c.c. lattice).

Equation (2) has a simplest form of free energy, which is used to model the kinetics of the system. However, we should mention that, in order to calculate the miscibility gap and the free energy, a more complicated expression should be used (see Appendix). The 'paramagnetic' energies, $\{w_{\text{prm}}(\mathbf{r})\}$, are calculated, considering the polynomial approximation proposed in Refs. [5, 9]. Besides, for a magnetic alloy, one should also consider spin-dynamics equations, *i.e.* it is necessary to take into account the nonzero derivatives of relative magnetizations, $\{d\sigma_\alpha(\mathbf{r},t)/dt\}$. However, as, for considered Ni–Fe alloys, the spin-rotation relaxation rate is much higher than the rates of atomic microdiffusion jumps, these terms are neglected in the presented model. Therefore, the magnetic contribu-

tion to the overall system evolution consists of adding the magnetic energies ($w_{\text{magn}}(\mathbf{r}) = J^{\text{FeFe}}(\mathbf{r}) s_{\text{Fe}}^2 \sigma_{\text{Fe}}^2 + J^{\text{NiNi}}(\mathbf{r}) s_{\text{Ni}}^2 \sigma_{\text{Ni}}^2 - 2J^{\text{NiFe}}(\mathbf{r}) s_{\text{Fe}} s_{\text{Ni}} \sigma_{\text{Fe}} \sigma_{\text{Ni}}$ within the intracrystalline 'molecular field' approximation that is the mean self-consistent-field one) to the total 'mixing' energies of constituents described with the spin numbers, $\{s_\alpha\}$, 'coupled' by means of the 'exchange integrals', $\{J^{\alpha\beta}(\mathbf{r})\}$. The equilibrium values of $\{\sigma_\alpha\}$ are found by minimization of the total free energy (see Refs. [5, 9, 15, 16] and Appendix), accounting a magnetic contribution to the entropy too.

The elastic energy, which arises from the mismatch between the lattice parameters of the matrix and the precipitates of a new phase, can be calculated within the scope of the Khachaturyan–Shatalov microscopic elasticity theory of structurally inhomogeneous systems [12, 13, 17, 18]. Following Khachaturyan and colleagues [14, 19–23], the strain-induced energy generated by arbitrary structure inhomogeneity can be presented in terms of the concentration or long-range order parameter fields. Assuming the Végard's law and the equivalency of elastic moduli tensors, $\{\lambda_{ijkl}\}$, for host-crystal and precipitate phases, the morphology-dependent part of the strain-induced energy can be written in the reciprocal-space representation form as follows:

$$\Delta E_{\text{elast}} \approx \frac{\upsilon_0}{2N} \sum_{\mathbf{k} \in BZ} \tilde{B}(\mathbf{n}) \left| \tilde{C}(\mathbf{k}) \right|^2, \tag{4}$$

where $\mathbf{n} = \mathbf{k}/|\mathbf{k}|$ is a unit vector along the $\mathbf{k}$ direction, $\tilde{C}(\mathbf{k})$ is the Fourier transform of the inhomogeneous composition field, $c(\mathbf{r})$. The function $\tilde{B}(\mathbf{n}) = \varepsilon_0^2(\lambda_{iill} - n_i \lambda_{ijmm} \Omega_{jk}(\mathbf{n}) \lambda_{klm'm'} n_l)$ contains all information on the elastic properties of the system and crystallography of the phase precipitation, where $\upsilon_0^{-2}|\mathbf{k}|^{-2}\|\Omega_{ij}(\mathbf{n})\|$ is the Green function matrix asymptotics (at $\mathbf{k} \to \mathbf{0}$), which is inverse to the tensor $|\mathbf{k}|^2\|\Omega_{ij}(\mathbf{n})\|^{-1} = |\mathbf{k}|^2\|\lambda_{iklj} n_k n_l\|$; $\varepsilon_0 = (a_\gamma - a_\gamma)/\{a_\gamma(c_\beta^{(\gamma)} - c_\beta^{(\gamma)})\}$ is the concentration coefficient of stress-free lattice-transformation dilatation caused by the changes in composition of a binary alloy (υ_0 is the atomic volume); $c_\beta^{(\gamma)}$ ($c_\beta^{(\gamma)}$) and a_γ (a_γ) are the concentration of the solute and lattice parameter of f.c.c. disordered-matrix (ordered-precipitate) phase, respectively. At $\mathbf{k} = \mathbf{0}$, the function $\tilde{B}(\mathbf{n})$ has a singularity, since its limit at $\mathbf{k} \to \mathbf{0}$ depends on the $\mathbf{k}$ vector direction. This singularity results in a long-range asymptotic behaviour of the strain-induced interaction in a real space [24].

3. RESULTS AND DISCUSSION

The microstructure evolution is modelled on a $2D$ square lattice consisting of 1024×1024 unit cells. The nucleation stage is neglected as we limit ourselves to the study of the coarsening stage. Therefore, at the beginning of the simulation, from 200 to 800 small spherical precipitates of the new phase are manually embedded into the homogeneous

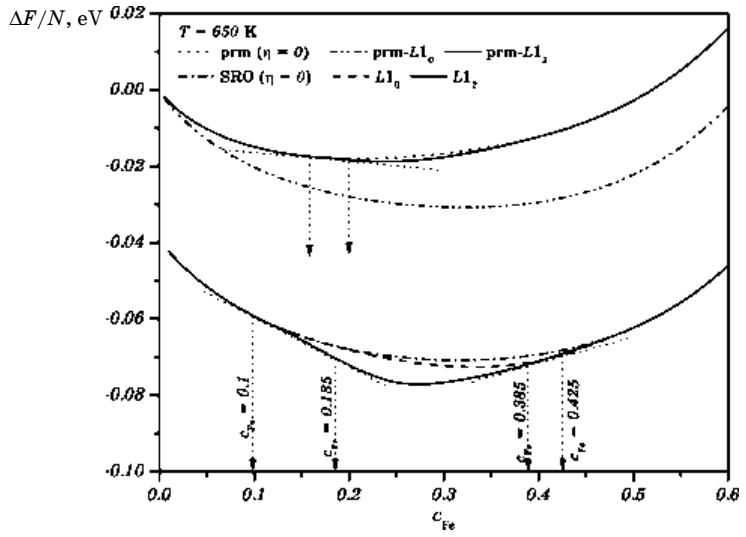

Fig. 2. The concentration dependence of the configuration part of the total free energy at $T = 650$ K.

matrix. The concentration of these precipitates is chosen, according to the equilibrium concentration of the ordered phase. The effects of magnetic and elastic contributions on the microstructure evolution are studied by comparison of simulations with and without the respective terms (w_{magn}, ΔE_{elast}) in the total 'mixing' energies of atoms and the free energy. The kinetic equation (1) is numerically solved in the reciprocal space by means of the explicit Euler method. The corresponding atomic distributions are recovered, using the backward Fourier transform. In the course of simulations, the periodic boundary conditions are applied, and the time step is set to $\Delta t = 10^{-5}$.

According to Fig. 1, the temperature $T = 650$ K is chosen in order to study the system in two-phase coexistence regions. Such a choice is confirmed by the thermodynamic calculations and the free energy plot (Fig. 2). In Figure 2, the two-phase regions (with $c_{\text{Fe}} \in [0.1; 0.185]$ for $L1_2 + A1$ mixture and $c_{\text{Fe}} \in [0.385; 0.425]$ for $L1_2 + L1_0$ one, respectively) are defined by the common tangent construction. From such a plot, one can notice that taking into account magnetic interactions leads to decrease of the total free energy and broadening of the phase boundaries, which testifies that magnetism stipulates the ordering processes and the stabilization of the ordered phases in the studied alloys. The investigation of kinetics should give further confirmation of such a hypothesis.

Simulations are performed for some representative compositions within the specified two-phase regions. In particular, $c_{\text{Fe}} = 0.14$ and 0.41 are chosen to study Permalloy and Elinvar alloys, respectively. The interaction parameters calculated at such thermodynamic condi-

TABLE 1. The interaction parameters ('mixing' energies) [meV] calculated at $T = 650$ K, considering that $w(\mathbf{r}_3) = 0.3$ meV and $w(\mathbf{r}_4) = 0.7$ meV [5, 9]. In the second column, the symbols '+' and '–' denote the presence and absence of magnetism.

c_{Fe}	magnetism	σ_{Ni}	σ_{Fe}	$\tilde{w}(\mathbf{k}_\Gamma)$	$\tilde{w}(\mathbf{k}_X)$	$w(\mathbf{r}_1)$	$w(\mathbf{r}_2)$
0.14	–	–	–	591.125	–351	58.283	–20.645
	+	0.767	0.806	854.048	–438.667	80.195	–20.648
0.41	–	–	–	313.255	–229.5	33.322	–17.035
	+	0.88	0.634	515.024	–296.778	50.138	–17.038

tions are listed in Table 1. The values for 1st and 2nd coordination shells are extracted from $\tilde{w}(\mathbf{k}_\Gamma)$ and $\tilde{w}(\mathbf{k}_X)$, using the set of linear equations:

$$\begin{cases} \tilde{w}(\mathbf{k}_\Gamma) \cong 12w(\mathbf{r}_1) + 6w(\mathbf{r}_2) + 24w(\mathbf{r}_3) + 12w(\mathbf{r}_4), \\ \tilde{w}(\mathbf{k}_X) \cong -4w(\mathbf{r}_1) + 6w(\mathbf{r}_2) - 8w(\mathbf{r}_3) + 12w(\mathbf{r}_4), \end{cases} \quad (5)$$

and considering the 'strain-induced' interactions right up to 4th shell ($w(\mathbf{r}_3) = 0.3$ meV, $w(\mathbf{r}_4) = 0.7$ meV; see details in [5, 9]); the 'paramagnetic' and magnetic interactions are considered as short-range ones, *i.e.* within the nearest (for magnetic) and next-nearest (for 'paramagnetic') neighbourhood only.

3.1. The Effect of Magnetism on the Microstructure

In Figure 3, the results of simulation are presented for both alloys: $Ni_{0.86}Fe_{0.14}$ Permalloy (Fig. 3, *a*) and $Ni_{0.59}Fe_{0.41}$ Elinvar (Fig. 3, *b*).

In order to clarify the role of magnetism in the ordered-structure formation in Permalloy alloys, two kinds of simulations are performed: with neglecting magnetic contribution, *i.e.* $w_{magn} \equiv 0$, and with considering it *via* the appropriate calculation of $w_{magn} \neq 0$. In both cases, the initial configuration of an alloy is consisted of disordered matrix with $c_{Fe} = 0.1$ and a set of small $L1_2$-ordered nuclei with $c_{Fe} = 0.185$. The time evolution of a nonconserved system that separates into phases of different concentration is studied and shown in Fig. 3, *a* at reduced time $t^* = \{0, 20, 40\}$ (measured in units of Monte Carlo steps per site [MCS/s]).

Neglecting the magnetic nature of an alloy ($w_{magn} \equiv 0$; Fig. 3, *a*, left column) results in complete disappearance of the nuclei of ordered phase, which were initially embedded into the disordered matrix. This behaviour agrees with the calculated configuration-dependent free energy curves (Fig. 2) and testifies that, at such temperature and at the condition of $w_{magn} \equiv 0$, the chosen alloy does not undergo an ordering reaction.

In turn, *taking into account the magnetic effects*, one obtains an opposite result. During the evolution, the growth and coarsening stages

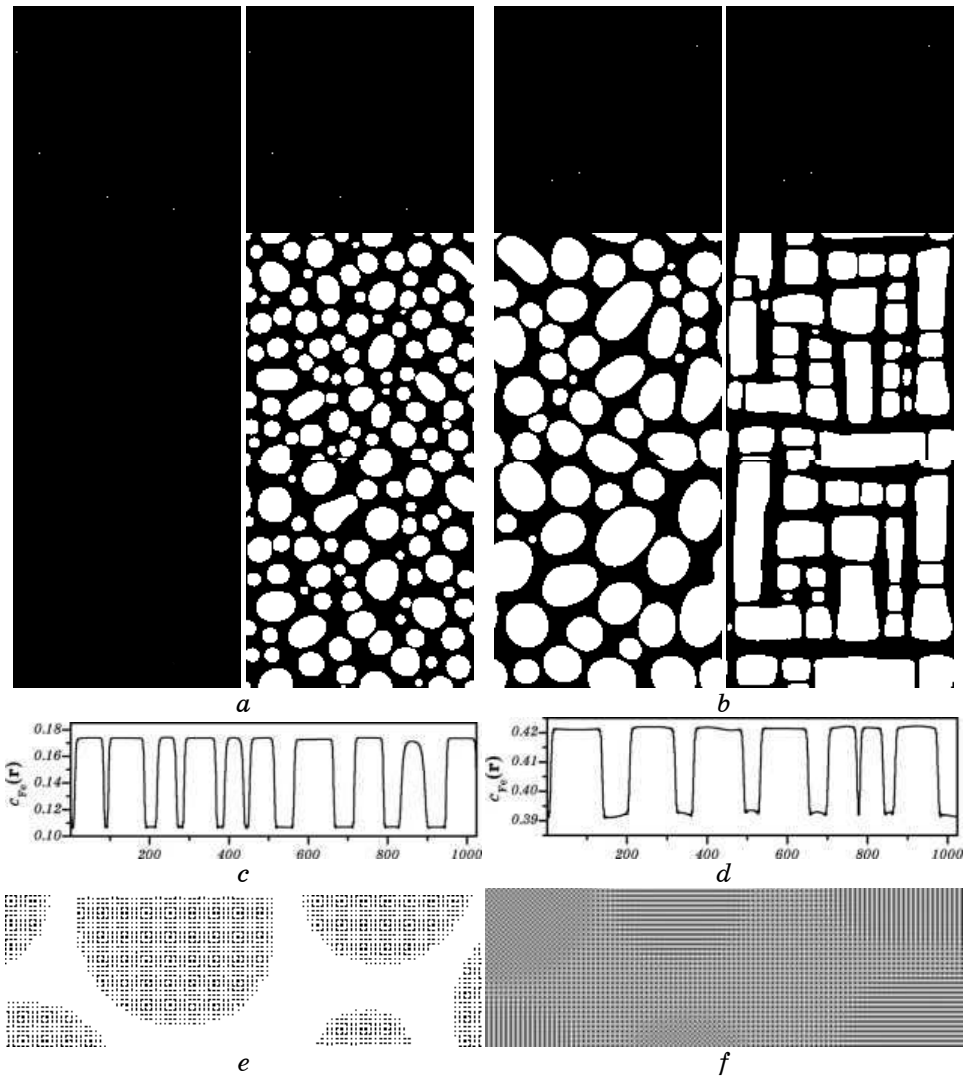

Fig. 3. The microstructure evolution of $Ni_{0.86}Fe_{0.14}$ Permalloy (*a*) and $Ni_{0.59}Fe_{0.41}$ Elinvar (*b*) alloys at reduced time $t^* = \{0, 20, 40\}$ with (right columns) and without (left columns) taking into account the magnetic (*a*) and elastic (*b*) effects; (*c*), (*d*)—respective concentration profiles and (*e*), (*f*)—atomic arrangements corresponding to medium section at $t^* = 40$.

appear sequentially, and at late stages, the large $L1_2$-ordered precipitates continue to coarsen the smaller ones until the stationary state is attained.

The morphology of the obtained structure allows to clearly distinguish both $A1$-type disordered phase and $L1_2$-type ordered one (marked

with black and white colours in Fig. 3, *a* (right column), respectively).

The latter forms the precipitates of nearly spherical shape. At late stages of evolution, the system is characterised by a set of the ordered particles, which differ from each other by a displacement vector ((011)$a/2$, (101)$a/2$ or (110)$a/2$) and are separated by the antiphase (APB) and interphase (IPB) boundaries.

We should note that, for larger Fe content (closer to the right limit of the two-phase coexistence interval, *e.g.*, $c_{\mathrm{Fe}}=0.17$), the ordered phase grows till the size of large domains, and the main evolution mechanisms in this case will be as follow: 1) the growth of large domains at the expense of the APB movement, 2) the merging of two domains of the same type, and 3) the dissolution of the intermediate domains (see Ref. [25] and references therein).

In Figure 3, *c*, the local concentration profile for the longitudinal median section of final structure at $t^{*}=40$ for simulated $\mathrm{Ni}_{0.86}\mathrm{Fe}_{0.14}$ Permalloy is presented. Let us note that the local concentration at each lattice site is calculated by means of averaging over the 1st and 2nd coordination shells [14, 19–22, 25–27]. As can be seen, in the disordered phase, the local concentration approaches the equilibrium concentration of the disordered phase determined by the phase diagram (Fig. 2), *i.e.* $c_{\mathrm{Fe}}\approx 0.1$. In turn, the ordered phase is characterised by the local concentration $c_{\mathrm{Fe}}\approx 0.176$ and tends to the equilibrium concentration of the $L1_2$-type phase, *i.e.* 0.185.

The example of atomic configuration for simulated $\mathrm{Ni}_{0.86}\mathrm{Fe}_{0.14}$ Permalloy at late stage of evolution ($t^{*}=40$) is presented in Fig. 3, *e*. The black (white) colour marks the lattice sites, where the Fe (Ni) atoms can be found with the highest probability; grey colour marks the sites, where the probabilities to find Fe (Ni) atoms are identical, *i.e.* the disordered phase. Inside the ordered precipitates, the atoms alternate in the manner inherent to the $2D$ projection of the $L1_2$-type superstructure.

3.2. The Effect of Elastic Contribution on the Microstructure

The influence of the elastic energy on the microstructure of the Elinvar alloys is studied by means of two kinds of simulations: neglecting the elastic term (Eq. (4)), *i.e.* $\Delta E_{\mathrm{elast}}\equiv 0$, and considering it by the explicit calculation of $\Delta E_{\mathrm{elast}}\neq 0$. In both cases, the initial configuration of the alloy consisted of both $L1_2$-type ordered matrix with $c_{\mathrm{Fe}}=0.385$ and a set of small $L1_0$-type ordered nuclei with $c_{\mathrm{Fe}}=0.425$. The time evolution of a nonconserved system at issue at reduced times $t^{*}=\{0, 20, 40\}$ is shown in Fig. 3, *b*. Let us mention that, for Elinvar alloys, it is important to consider the elastic contribution, $\Delta E_{\mathrm{elast}}$, to the free-energy functional due to the tetragonality of $L1_0$-type phase and more pronounced crystal-lattice mismatch between the two adjacent phases ($L1_2$ and $L1_0$) than in Permalloys ($L1_2$ and $A1$). Owing to the small difference in the tetragonal-phase

parameters, a and b, [28, 29], in the presented simulations, this feature is neglected, and the following lattice parameters are used [1, 29]: $a_{A1} \approx 0.35338$ nm, $a_{L1_2} \approx 0.356667$ nm, $a_{L1_0} \approx 0.358229$ nm.

One should mention that, for Elinvar alloys, the role of magnetic contribution is also tested, and the obtained results resemble the outcomes reported above for the Permalloy alloys. Neglecting the magnetism results in dissolution of the embedded nuclei. Thus, further, the magnetic contribution will be implied by default and, as seen from Fig. 3, *b*, the microstructure formation is a result of the growth and coarsening stages. When *elastic energy is neglected* (Fig. 3, *b*, left column), the obtained microstructure contains precipitates of nearly spherical shape, which are isotropically distributed over the system.

However, *taking into account the elastic energy* (in particular, due to the elastic interactions between the $L1_0$-type precipitates) results in both change of precipitates shape to the plate-like (or rectangular) one and the anisotropy along $(100)^*$ direction in their distribution. Let us note that the appearance of the anisotropy in the system with $L1_0$-type order has been found previously (see Refs. [19, 20, 22, 25] and references therein), but as shown, it appears along the $(110)^*$-type direction, and the precipitates form a certain type of pattern, for instance, tweed, twin, chessboard-like patterns, *etc.* We assume that such behaviour is a consequence of the tetragonality of $L1_0$-type phase, and, as we have neglected this feature in our simulation, we do not expect the identical peculiarities.

Among the specific features of the microstructure generated, considering the elastic effects (ΔE_{elast}), one can note the formation of 'chains' of precipitates, which appear due to inability of particles with different orientation and translation variants to merge (coalesce). (In general, in $3D$ case, the precipitates of $L1_0$-type phase have three orientation variants and three translation variants, *i.e.* in total, six variants; in $2D$ case, one has three different variants). For visual presentation of the microstructure, which is formed during the evolution, the local concentration profile for the longitudinal median section and the example of atomic configuration of final structure at $t^* = 40$ for simulated $Ni_{0.59}Fe_{0.41}$ Elinvar are shown in Fig. 3, *d* and *f*, respectively. In the latter figure, one can clearly see the precipitates of $L1_0$-type phase of three different types (the atoms are altered in a different manner) and the $L1_2$-type phase matrix. The black (white) colour marks the lattice sites, where the Fe (Ni) atoms can be found with the highest probability. As seen in Figure 3, *d*, the local concentration profile smears out approaching the IPB owing to the change of ordered structure; the APB between the precipitates are not found as a result of wetting by $L1_2$ phase.

3.3. Analysis of the Microstructure Evolution

The shape of precipitates can be estimated by the *aspect ratio* (AR) of

their sides in 0x and 0y directions following the rules: if AR < 1.5, precipitates have a shape close to circle (spherical) or square (cubical); if 1.5 < AR < 2.5, particles possess a rectangle shape; if 2.5 < AR < 3.5 or AR > 3.5, precipitates tend to have a plate-like shape [30]. One can see in Fig. 4, *a* that such an analysis adequately reflects the simulated shapes of precipitates: for $Ni_{0.86}Fe_{0.14}$ Permalloy and $Ni_{0.59}Fe_{0.41}$ Elinvar without elastic contribution, the AR tends to unity that confirms a spherical shape of precipitates; in turn, considering the elastic contribution for $Ni_{0.59}Fe_{0.41}$ Elinvar, the AR is evidently > 1.5 and < 2.5, confirming a rectangular shape.

In Figure 4, *b*, the calculated volume fraction of a new phase is shown for all simulated alloys. When magnetic interactions are neglected, the dissolution of all particles of the $L1_2$-type ordered phase results in a fast decrease (to 0) of a volume fraction, and therefore, further analysis of this case will be omitted. During the growth regime, the volume fraction of $Ni_{0.86}Fe_{0.14}$ Permalloy (with magnetic effects) grows from 0.004 to 0.5 and reaches its equilibrium value already at $t^* \approx 1$ that indicates

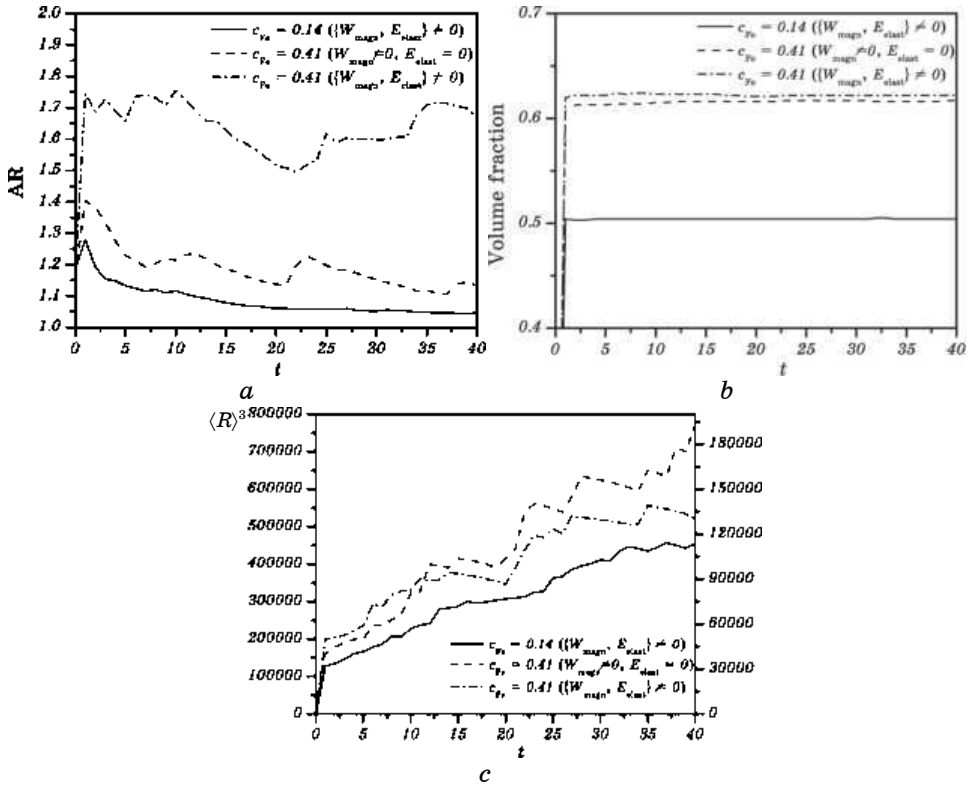

Fig. 4. The time evolution of the aspect ratio, AR (*a*), volume fraction (*b*) and cube of the average precipitate radius (*c*) for $Ni_{0.86}Fe_{0.14}$ and $Ni_{0.59}Fe_{0.41}$ alloys.

the start of the coarsening regime. Similarly, the volume fraction of $Ni_{0.59}Fe_{0.41}$ Elinvars indicates the start of coarsening regime already at $t^* \approx 1$ and reaches 0.617 and 0.622, when elastic effects are neglected and taken into account, respectively. Such a difference can be attributed to the different number of precipitates contained in the system at different time intervals; for example, at last time step ($t^* \approx 40$), the studied alloy has 22 and 26 $L1_0$-type particles, respectively.

Following the Lifshitz–Slyozov and Wagner's theory (LSW, [31, 32]), at late stages of evolution, the *cube of the average particle radius* obeys a power law:

$$\langle R \rangle^3 \propto Kt\,, \tag{6}$$

where $\langle R \rangle$ is an average radius of a precipitate, t is a time of rise, K is the coarsening rate. In Figure 4, *c*, such behaviour is noticeable for all studied alloys. A slope of each curve determines the coarsening rate, K. One can also visually distinguish the growth and coarsening stages; at the growth stage, the radius of particles grows very fast and, therefore, the slope of the curves is steepest. From the simulated data, one can estimate the average size of precipitate, and using the linear approximation, one can estimate the coarsening rate as a slope of the respective linear curve, $Kt + \text{const} \cong \langle R \rangle^3$. For $Ni_{0.86}Fe_{0.14}$ Permalloy, one finds $\langle R \rangle \approx 8.6$ nm (at $t^* \approx 40$) and $K \approx 2309.52$ (in arbitrary units). The same analysis can be applied to the outcomes for $Ni_{0.59}Fe_{0.41}$ Elinvar; the effect of the elastic contribution can be seen in a slowing down the coarsening reaction and a respective decay of the $\langle R \rangle^3(t)$ curve.

The fluctuating character of the $<R>^3(t)$ dependences for Elinvar alloy is explained by a small amount of precipitates at the late stages of evolution; the averaging over a number of different system realizations (initial precipitates' amount and distribution) can possibly smooth the resulting curve. (In particular, the results in Fig. 4 are obtained after averaging over different precipitates' distributions with their initial number equal to 200 and 800.)

The classical LSW theory also predicts a specific time-independent form of a precipitates' *size distribution* (see the thick grey curve on Fig. 5, *a*, *b*), but as seen for all simulated alloys, the size distribution curves appreciably deviate. For $Ni_{0.86}Fe_{0.14}$ Permalloy (Fig. 5, *a*), one can deduce the asymptotic form of the curves for the precipitation of particles of some characteristic size, namely, the features inherent to the classical LSW theory. But, owing to the considerable volume fraction of the precipitated phase, the form of the curve deviates from the classical one, namely, one can notice the broadening, the more symmetrical shape of a distribution, and a shift of the maximum to the region of sizes, which are smaller than the average precipitates' radius, $<R>$. At late stage ($t^* = 40$), the distribution widens towards the range of big-particle

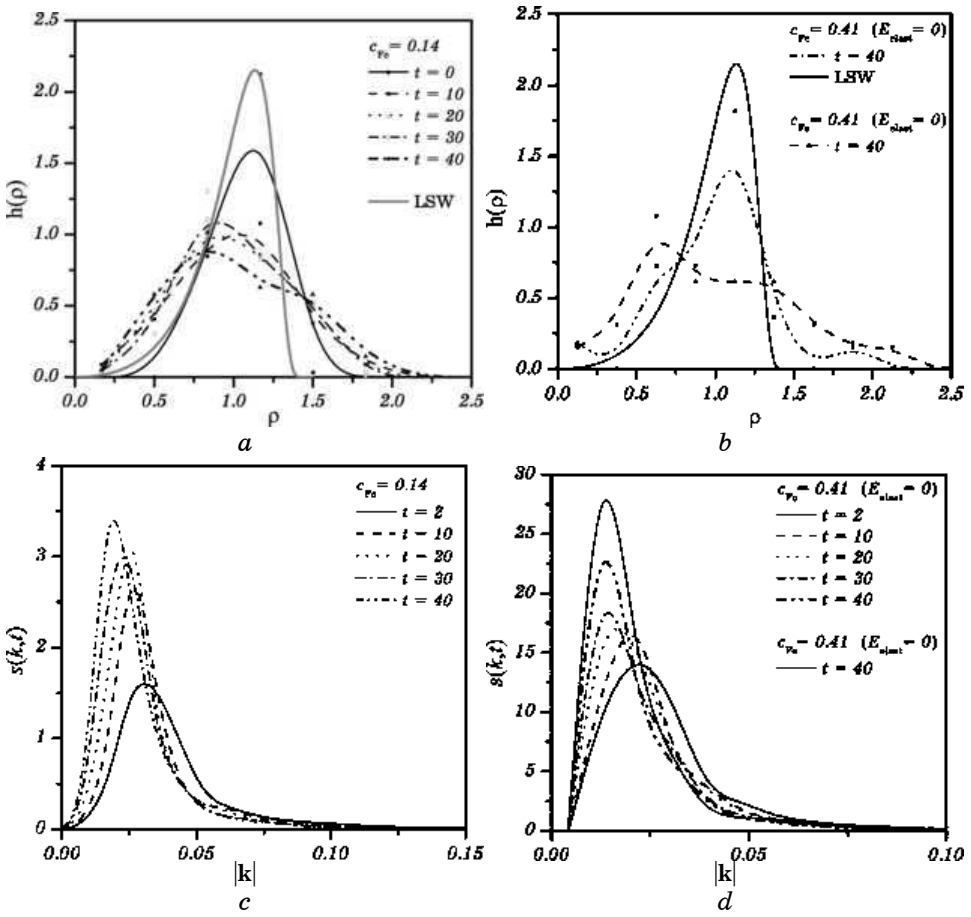

Fig. 5. The time evolution of the size distribution function, $h(\rho)$ ($\rho = \langle R \rangle / R$), (*a*, *b*) and the structure factor (*c*, *d*) for $Ni_{0.86}Fe_{0.14}$ and $Ni_{0.59}Fe_{0.41}$, respectively.

sizes that confirms the increase of larger particles comparing to the previous evolution stages; the distribution has the 'tails' that signifies the presence of the precipitates (domains) with a size much greater than the average $\langle R \rangle$. In case of $Ni_{0.59}Fe_{0.41}$ Elinvar, the size distribution also deviates from its classical form (Fig. 5, *b*), and one can see that taking into account the elastic effects changes its form. In particular, when $\Delta E_{\text{elast}} \neq 0$, the distribution broadens, and the maximum shifts to the range of smaller precipitate sizes. Similar to the Permalloy, the Elinvar distribution curves allow one to distinguish a significant amount of precipitates with a size much greater than the average $\langle R \rangle$.

The deviation of the distribution curves from the classical LSW relation due to the considerable (not null) volume fraction has been reported previously and generated a number of investigations concerned

with its improvement and modification (see, for example, [33–35]). For instance, according to the modified LSW theory (LSEM—Lifshitz–Slyozov encounter modified one [35]), the widening of the distribution takes place at the expense of the removal of two small particles and the addition of one big particle instead (see also Ref. [27]).

Another quantity, which allows drawing a conclusion about the order and the scale of the obtained structure, is the structure factor, which is a Fourier transform of a pair-correlation function:

$$S(\mathbf{k},t)=\left\langle \frac{1}{N}\sum_{\mathbf{r}}\sum_{\mathbf{r}'} e^{-i\mathbf{k}\cdot\mathbf{r}}\left(c(\mathbf{r}',t)c(\mathbf{r}+\mathbf{r}',t)-c_{\mathrm{Fe}}^2\right)\right\rangle, \tag{7}$$

where $c(\mathbf{r})$ is a local concentration at the site $\mathbf{r}$ at the instant of time t, c_{Fe} is a nominal concentration of the alloy, $\mathbf{k}$ is a wave vector within the 1st Brillouin zone of the reciprocal space. The sum and average ($\langle\ldots\rangle$) is taken over all N crystal-lattice sites. Further, it is more convenient to use the normalized spherically averaged structure factor:

$$s(k,t)=\frac{S(k,t)}{\sum\limits_{\mathbf{k}} S(\mathbf{k},t)}=\frac{S(k,t)}{N\left(\left\langle c^2(\mathbf{r})\right\rangle-c_{\mathrm{Fe}}^2\right)}. \tag{8}$$

$S(k,t)=\dfrac{\sum\limits_{k-\Delta k/2<|\mathbf{k}|\le k+\Delta k/2} S(\mathbf{k},t)}{\sum\limits_{k-\Delta k/2<|\mathbf{k}|\le k+\Delta k/2} 1}$ is a spherically averaged structure factor, where $k=|\mathbf{k}|$ is a length of the wave vector $\mathbf{k}$. In the denominator, there is a number of points lying in the Δk-thickness vicinity of the wave vector $\mathbf{k}$. The time evolutions of the calculated structure factors for $Ni_{0.86}Fe_{0.14}$ and $Ni_{0.59}Fe_{0.41}$ are shown in Fig. 5, *c*, *d*, respectively. As can be seen from both graphs, the width of structure factor reduces with time that evidences the formation of sharp interface between two phases ($L1_2+A1$ and $L1_2+L1_0$, respectively); the maximum height increases and shifts to lower $\mathbf{k}$ values confirming thereby the coarsening reactions and the increase of the precipitates' size [27, 30, 36, 37]. The elastic contribution (Fig. 5, *d*) does not influence the location of the maximum but slightly increases its height and width. The broadening of the maximum and the respective smearing of IPB is confirmed by the local concentration profile (Fig. 3, *d*), which is diffuse close to IPB, and by the appearance of 'chains' of precipitates situated close to each other. In this case, the IPB can be very narrow (up to 2 interatomic distances) and diffuse. For $Ni_{0.59}Fe_{0.41}$ with $\Delta E_{\mathrm{elast}}\equiv 0$, the number of such IPB is smaller.

Let us mention that the structure factor can be evaluated experimentally due to its straightforward connection to the coherent scattering intensity. Thus, the conclusions drawn from the computer simula-

tions can be confirmed by the investigation of the real alloy samples.

4. CONCLUSION

In a given article, the physical kinetics of the atomic orders in Permalloy and Elinvar alloys is investigated, using the Onsager-type microdiffusion equation. A special attention is paid to the effects generated by the magnetic and elastic interactions in these alloys. As revealed, the magnetic nature substantially influences the atomic ordering in this system and, in fact, promotes to stabilize the ordered phase ($L1_2$ in Permalloys and $L1_0$ in Elinvars) and increases the width of the two-phase coexistence region. In turn, the elastic interactions between the precipitates significantly change the morphology of the Elinvar alloys, promoting the anisotropy in the form and the arrangement of precipitates. For Permalloy alloys, the elastic effects turn out to be negligible.

The calculated statistical characteristics confirm the effects of magnetic and elastic interactions on the kinetics and structure properties. The simulated microstructure for the high volume fraction of $L1_2$ phase is in a good agreement with the available experimental data [11]. One should also note that, due to the slow diffusion processes in f.c.c.-Ni–Fe alloys and low temperatures of the order–disorder phase transition, there are only a few experimental data about the microstructure in these nonconserved systems. The latter makes the presented study useful for a general consideration of magnetically and atomically ordered systems.

ACKNOWLEDGEMENTS

The authors express their appreciation to Dr. H. M. Zapolsky and Prof. D. Ledue (GPM, UMR 6634 CNRS, Université de Rouen, France) for very constructive discussion of the results obtained in the course of a given work. We are grateful to Prof. B. Schönfeld (ETH, Switzerland) and Prof. S. Hata (Kyushu University, Japan) for stimulating discussions on atomic ordering phenomena in metallic alloys. I.V.V. acknowledges the UMR 6634 (France) for partial financial support of a given work. S.M.B. would like to thank also the Institute for Advanced Materials Science and Innovative Technologies (Lithuania) for partial financial support of a given work.

APPENDIX A

The free energy and the phase diagram can be calculated, using the SCW representation [12, 13], where the occupation probabilities $\{p(\mathbf{r})\}$ are defined as follow:

$$p(\mathbf{r}) = c_\beta + \frac{\eta}{4}\left[e^{i2\pi\mathbf{a}_1^*\cdot\mathbf{r}} + e^{i2\pi\mathbf{a}_2^*\cdot\mathbf{r}} + e^{i2\pi\mathbf{a}_3^*\cdot\mathbf{r}}\right] \tag{A1}$$

for $L1_2$-type superstructure and

$$p(\mathbf{r}) = c_\beta + \frac{\eta}{2} e^{i2\pi\mathbf{a}_3^*\cdot\mathbf{r}} \tag{A2}$$

for $L1_0$-type superstructure, respectively. η is the long-range order parameter, which varies from 0 in the disordered state to 1 in the completely ordered state (at the corresponding stoichiometry); the vectors $\mathbf{a}_1^*$, $\mathbf{a}_2^*$, $\mathbf{a}_3^*$ are the unit reciprocal-lattice vectors of f.c.c. crystal lattice along [100], [010] and [001] directions, respectively; $|\mathbf{a}_1^*|=|\mathbf{a}_2^*|=|\mathbf{a}_3^*|= =1/a$. Substituting Eqs. (A1), (A2) into Eq. (2), the expression for the 'paramagnetic' free energy of the $L1_2$-type structure can be written as:

$$\begin{aligned}\frac{\Delta F}{N} \cong\ & \frac{1}{2}c_\beta^2\tilde{w}_{\text{prm}}(\mathbf{0}) + \frac{3}{2}\left(\frac{\eta}{4}\right)^2\tilde{w}_{\text{prm}}(\mathbf{k}_X) + \\ & + \frac{k_B T}{4}\left\{\begin{array}{l} 3\left(c_\beta - \frac{\eta}{4}\right)\ln\left(c_\beta - \frac{\eta}{4}\right) + 3\left(1 - c_\beta + \frac{\eta}{4}\right)\ln\left(1 - c_\beta + \frac{\eta}{4}\right) + \\ + \left(c_\beta + \frac{3}{4}\eta\right)\ln\left(c_\beta + \frac{3}{4}\eta\right) + \left(1 - c_\beta - \frac{3}{4}\eta\right)\ln\left(1 - c_\beta - \frac{3}{4}\eta\right)\end{array}\right\},\end{aligned} \tag{A3}$$

where c_β is the solute concentration.

The magnetic free energy can be defined within the scope of the 'molecular field' approximation [5, 7, 9, 10, 13], and the resulting configuration-dependent part of the total free energy will have a form:

$$\begin{aligned}\frac{\Delta F}{N} \cong\ & \frac{1}{2}\Big[c_\beta^2\tilde{w}_{\text{prm}}(\mathbf{0}) + \tilde{J}^{\alpha\alpha}(\mathbf{0})\sigma_\beta^2 s_\beta^2 c_\beta^2 + \tilde{J}^{\beta\beta}(\mathbf{0})\sigma_\alpha^2 s_\alpha^2 (1-c_\beta)^2 + 2\tilde{J}^{\alpha\beta}(\mathbf{0})\sigma_\alpha\sigma_\beta s_\alpha s_\beta c_\beta(1-c_\beta) + \\ & + \frac{3}{16}\eta^2\left(\tilde{w}_{\text{prm}}(\mathbf{k}_X) + \tilde{J}^{\alpha\alpha}(\mathbf{k}_X)\sigma_\alpha^2 s_\alpha^2 + \tilde{J}^{\beta\beta}(\mathbf{k}_X)\sigma_\beta^2 s_\beta^2 - 2\tilde{J}^{\alpha\beta}(\mathbf{k}_X)\sigma_\alpha\sigma_\beta s_\alpha s_\beta\right)\Big] + \\ & + \frac{k_B T}{4}\left\{\begin{array}{l}\left(c_\beta + \frac{3}{4}\eta\right)\ln\left(c_\beta + \frac{3}{4}\eta\right) + \left(1 - c_\beta - \frac{3}{4}\eta\right)\ln\left(1 - c_\beta - \frac{3}{4}\eta\right) + \\ + 3\left(c_\beta - \frac{\eta}{4}\right)\ln\left(c_\beta - \frac{\eta}{4}\right) + 3\left(1 - c_\beta + \frac{\eta}{4}\right)\ln\left(1 - c_\beta + \frac{\eta}{4}\right)\end{array}\right\} - \\ & - k_B T\left\{c_\beta\left[\ln\left(\text{sh}\left(\frac{(2s_\beta+1)y_\beta(\sigma_{\beta,\alpha})}{2s_\beta}\right)\right) - \ln\left(\text{sh}\left(\frac{y_\beta(\sigma_{\beta,\alpha})}{2s_\beta}\right)\right) - y_\beta(\sigma_{\beta,\alpha})B_{s_\beta}(y_\beta(\sigma_{\beta,\alpha}))\right] + \right. \\ & \left. + (1-c_\beta)\left[\ln\left(\text{sh}\left(\frac{(2s_\alpha+1)y_\alpha(\sigma_{\alpha,\beta})}{2s_\alpha}\right)\right) - \ln\left(\text{sh}\left(\frac{y_\alpha(\sigma_{\alpha,\beta})}{2s_\alpha}\right)\right) - y_\alpha(\sigma_{\alpha,\beta})B_{s_\alpha}(y_\alpha(\sigma_{\alpha,\beta}))\right]\right\}\end{aligned} \tag{A4}$$

for $L1_2$-type phase (for Ni_3Fe alloys or for $NiFe_3$ alloys after a trivial

change of indexes: $\beta \leftrightarrow \alpha$);

$$\frac{\Delta F}{N} \cong$$

$$\cong \frac{1}{2}\Big[c_\beta^2 \tilde{w}_{\text{prm}}(\mathbf{0}) + \tilde{J}^{\beta\beta}(\mathbf{0})\sigma_\beta^2 s_\beta^2 c_\beta^2 + \tilde{J}^{\alpha\alpha}(\mathbf{0})\sigma_\alpha^2 s_\alpha^2 (1-c_\beta)^2 + 2\tilde{J}^{\alpha\beta}(\mathbf{0})\sigma_\alpha \sigma_\beta s_\alpha s_\beta c_\beta (1-c_\beta) +$$

$$+\frac{1}{4}\eta^2 \left(\tilde{w}_{\text{prm}}(\mathbf{k}_X) + \tilde{J}^{\alpha\alpha}(\mathbf{k}_X)\sigma_\alpha^2 s_\alpha^2 + \tilde{J}^{\beta\beta}(\mathbf{k}_X)\sigma_\beta^2 s_\beta^2 - 2\tilde{J}^{\alpha\beta}(\mathbf{k}_X)\sigma_\alpha \sigma_\beta s_\alpha s_\beta \right) \Big] +$$

$$+\frac{k_B T}{2}\left(\begin{array}{l} \left(c_\beta + \frac{1}{2}\eta\right)\ln\left(c_\beta + \frac{1}{2}\eta\right) + \left(1 - c_\beta - \frac{1}{2}\eta\right)\ln\left(1 - c_\beta - \frac{1}{2}\eta\right) + \\ + \left(c_\beta - \frac{\eta}{2}\right)\ln\left(c_\beta - \frac{\eta}{2}\right) + \left(1 - c_\beta + \frac{\eta}{2}\right)\ln\left(1 - c_\beta + \frac{\eta}{2}\right) \end{array} \right) -$$

$$-k_B T \left\{ c_\beta \left[\ln\left(\text{sh}\left(\frac{(2s_\beta + 1) y_\beta(\sigma_{\beta,\alpha})}{2s_\beta} \right) \right) - \ln\left(\text{sh}\left(\frac{y_\beta(\sigma_{\beta,\alpha})}{2s_\beta} \right) \right) - y_\beta(\sigma_{\beta,\alpha}) B_{s_\beta}(y_\beta(\sigma_{\beta,\alpha})) \right] + \right.$$

$$\left. + (1 - c_\beta)\left[\ln\left(\text{sh}\left(\frac{(2s_\alpha + 1) y_\alpha(\sigma_{\alpha,\beta})}{2s_\alpha} \right) \right) - \ln\left(\text{sh}\left(\frac{y_\alpha(\sigma_{\alpha,\beta})}{2s_\alpha} \right) \right) - y_\alpha(\sigma_{\alpha,\beta}) B_{s_\alpha}(y_\alpha(\sigma_{\alpha,\beta})) \right] \right\} \tag{A5}$$

for $L1_0$-type phase (NiFe alloys). $\tilde{w}_{\text{prm}}(\mathbf{k})$ is the $\mathbf{k}$-th Fourier component of the 'paramagnetic' mixing energies $\{w_{\text{prm}}(\mathbf{r}-\mathbf{r}')\}$; $\tilde{J}^{\alpha\beta}(\mathbf{k})$ is the $\mathbf{k}$-th Fourier component of the magnetic 'exchange' interactions 'integrals' $\{J^{\alpha\beta}(\mathbf{r}-\mathbf{r}')\}$; $\sigma_\alpha(\sigma_\beta)$ is the magnetic long-range order parameter (*i.e.* the reduced magnetization of α (β) constituents); s_α (s_β) is the value of the total spin number of an atom of α (β) kind; $B_J(\zeta)$ is the conventional Brillouin function defined as follows:

$$B_{J_\alpha}(\zeta_\alpha) \equiv \left(1 + \frac{1}{2J_\alpha}\right)\text{cth}\left(\left(1 + \frac{1}{2J_\alpha}\right)\zeta_\alpha\right) - \frac{1}{2J_\alpha}\text{cth}\left(\frac{1}{2J_\alpha}\zeta_\alpha\right),$$

$$\zeta_\alpha \equiv \frac{J_\alpha H_{\text{mol}}^\alpha}{k_B T} \cong \frac{J_\alpha g \mu_B}{k_B T}\left(-\sum\nolimits_\beta \Gamma_{\alpha\beta}\sigma_\beta\right),$$

where $J_\alpha = s_\alpha + l_\alpha$ is the total angular moment of an atom, which consists of both the spin number (s_α) and the orbital momentum number (l_α). We assume that, for transition metals, $J_\alpha \cong s_\alpha$. $H_{\text{mol}}^\alpha \cong -g\mu_B \sum_\beta \Gamma_{\alpha\beta}\sigma_\beta$ is the Weiss intracrystalline 'molecular field' (MSCF) with coefficients $\{\Gamma_{\alpha\beta}\}$.

The equilibrium order parameters can be determined by solving the set of transcendental equations obtained after minimizing the free energy.

For $L1_2$-type superstructure, one obtains:

$$\begin{cases} \ln\dfrac{\left(c_\beta-\dfrac{\eta}{4}\right)\left(1-c_\beta-\dfrac{3}{4}\eta\right)}{\left(1-c_\beta+\dfrac{\eta}{4}\right)\left(c_\beta+\dfrac{3}{4}\eta\right)}=\dfrac{\eta}{k_BT}\left[\begin{matrix}\tilde{w}_{\text{prm}}(\mathbf{k}_X)+\tilde{J}^{\alpha\alpha}(\mathbf{k}_X)s_\alpha^2\sigma_\alpha^2+\\ +\tilde{J}^{\beta\beta}(\mathbf{k}_X)s_\beta^2\sigma_\beta^2-2\tilde{J}^{\alpha\beta}(\mathbf{k}_X)s_\alpha s_\beta\sigma_\alpha\sigma_\beta\end{matrix}\right], \\ \sigma_\alpha=B_{s_\alpha}\left(-\dfrac{1}{(1-c_\beta)k_BT}\left\{\begin{matrix}\tilde{J}^{\alpha\alpha}(\mathbf{0})(1-c_\beta)^2s_\alpha^2\sigma_\alpha+\tilde{J}^{\alpha\beta}(\mathbf{0})c_\beta(1-c_\beta)s_\alpha s_\beta\sigma_\beta+\\ +\dfrac{3}{16}\eta^2\left[\tilde{J}^{\alpha\alpha}(\mathbf{k}_X)s_\alpha^2\sigma_\alpha-\tilde{J}^{\alpha\beta}(\mathbf{k}_X)s_\alpha s_\beta\sigma_\beta\right]\end{matrix}\right\}\right), \\ \sigma_\beta=B_{s_\beta}\left(-\dfrac{1}{c_\beta k_BT}\left\{\begin{matrix}\tilde{J}^{\beta\beta}(\mathbf{0})c_\beta^2s_\beta^2\sigma_\beta+\tilde{J}^{\alpha\beta}(\mathbf{0})c_\beta(1-c_\beta)s_\alpha s_\beta\sigma_\alpha+\\ +\dfrac{3}{16}\eta^2\left[\tilde{J}^{\beta\beta}(\mathbf{k}_X)s_\beta^2\sigma_\beta-\tilde{J}^{\alpha\beta}(\mathbf{k}_X)s_\alpha s_\beta\sigma_\alpha\right]\end{matrix}\right\}\right); \end{cases} \tag{A6}$$

and for $L1_0$-type superstructure:

$$\begin{cases} \ln\dfrac{\left(c_\beta-\dfrac{\eta}{2}\right)\left(1-c_\beta-\dfrac{\eta}{2}\right)}{\left(1-c_\beta+\dfrac{\eta}{2}\right)\left(c_\beta+\dfrac{\eta}{2}\right)}=\dfrac{\eta}{k_BT}\left[\begin{matrix}\tilde{w}_{\text{prm}}(\mathbf{k}_X)+\tilde{J}^{\alpha\alpha}(\mathbf{k}_X)s_\alpha^2\sigma_\alpha^2+\\ +\tilde{J}^{\beta\beta}(\mathbf{k}_X)s_\beta^2\sigma_\beta^2-2\tilde{J}^{\alpha\beta}(\mathbf{k}_X)s_\alpha s_\beta\sigma_\alpha\sigma_\beta\end{matrix}\right], \\ \sigma_\alpha=B_{s_\alpha}\left(-\dfrac{1}{(1-c_\beta)k_BT}\left\{\begin{matrix}\tilde{J}^{\alpha\alpha}(\mathbf{0})(1-c_\beta)^2s_\alpha^2\sigma_\alpha+\tilde{J}^{\alpha\beta}(\mathbf{0})c_\beta(1-c_\beta)s_\alpha s_\beta\sigma_\beta+\\ +\dfrac{\eta^2}{4}\left[\tilde{J}^{\alpha\alpha}(\mathbf{k}_X)s_\alpha^2\sigma_\alpha-\tilde{J}^{\alpha\beta}(\mathbf{k}_X)s_\alpha s_\beta\sigma_\beta\right]\end{matrix}\right\}\right), \\ \sigma_\beta=B_{s_\beta}\left(-\dfrac{1}{c_\beta k_BT}\left\{\begin{matrix}\tilde{J}^{\beta\beta}(\mathbf{0})c_\beta^2s_\beta^2\sigma_\beta+\tilde{J}^{\alpha\beta}(\mathbf{0})c_\beta(1-c_\beta)s_\alpha s_\beta\sigma_\alpha+\\ +\dfrac{\eta^2}{4}\left[\tilde{J}^{\beta\beta}(\mathbf{k}_X)s_\beta^2\sigma_\beta-\tilde{J}^{\alpha\beta}(\mathbf{k}_X)s_\alpha s_\beta\sigma_\alpha\right]\end{matrix}\right\}\right). \end{cases} \tag{A7}$$

REFERENCES

1. G. Beranger, F. Duffault, J. Morlet, et J.-F. Tiers, *Les alliages de Fer et de Nickel. Cent ans apres le decouverte de l'Invar...* (Londres–Paris–New York: Lavoisier–Technique & Documentation: 1996).
2. *Binary Alloy Phase Diagrams* (Metals Park, CA: ASM: 1986), vol. **1**.
3. J. K. van Deen and F. van der Woude, *Acta Metall.*, **29**, No. 7: 1255 (1981).
4. R. J. Wakelin and E. L. Yates, *Proc. Phys. Soc. B*, **66**, No. 3: 221 (1953).
5. S. Bokoch and V. Tatarenko, *Solid State Phenomena*, **138**: 303 (2008).
6. I. V. Vernyhora, D. Ledue, R. Patte, and H. Zapolsky, *J. Magn. Magn. Mater*, **322**, No. 17: 2465 (2010).
7. A. Z. Menshikov and E. E. Yurchikov, *Izvestiya Akad. Nauk SSSR. Ser. Fiz.*, **36**, No. 7: 1463 (1972) (in Russian).

8. T. G. Kollie and C. R. Brooks, *phys. stat. sol. (a)*, **19**, No. 2: 545 (1973).
9. S. M. Bokoch and V. A. Tatarenko, *Uspehi Fiziki Metallov*, **11**, No. 4: 413 (2010).
10. I. V. Vernyhora, S. M. Bokoch, and V. A. Tatarenko, *Uspehi Fiziki Metallov*, **11**, No. 3: 313 (2010) (in Ukrainian).
11. D. G. Morris, G. T. Brown, R. C. Piller, and R. E. Smallman, *Acta Metall.*, **24**, No. 1: 21 (1976).
12. A. G. Khachaturyan, *Progr. Mat. Sci.*, **22**, No. 1: 1 (1978).
13. A. G. Khachaturyan, *Theory of Structural Transformations in Solids* (Minola, NY: Dover Publications: 2008).
14. Y. Wang, L.-Q. Chen, and A. G. Khachaturyan, *Acta Metall. Mater.*, **41**, No. 1: 279 (1993).
15. V. A. Tatarenko and T. M. Radchenko, *Intermetallics*, **11**, No. 11–12: 1319 (2003).
16. T. M. Radchenko and V. A. Tatarenko , *Uspehi Fiziki Metallov*, **9**, No. 1: 1 (2008) (in Ukrainian).
17. A. G. Khachaturyan, *Sov. Phys. Sol. State*, **8**, No. 9: 2163 (1967).
18. A. G. Khachaturyan and G. A. Shatalov, *Soviet. Phys. JETP*, **29**: 557 (1969).
19. Y. Le Bouar, A. Loiseau, and A. G. Khachaturyan, *Acta Mater.*, **46**, No. 8: 2777 (1998).
20. Y. Le Bouar and A. G. Khachaturyan, *Acta Mater.*, **48**, No. 8: 1705 (2000).
21. S. Semenovskaya and A. G. Khachaturyan, *Acta Mater.*, **45**, No. 10: 4367 (1997).
22. Y. Le Bouar and A. Loiseau, *Acta Mater.*, **49**, No. 14: 2679 (2001).
23. J. Zhu, L.-Q. Chen, and J. Shen, *Modelling Simul. Mater. Sci. Eng.*, **9**: 499 (2001).
24. A. G. Khachaturyan and G. A. Shatalov, *Sov. Phys. Solid State*, **11**: 118 (1969).
25. V. G. Vaks, *Phys. Rep.*, **391**, Nos. 3–6: 157 (2004).
26. L.-Q. Chen and A. G. Khachaturyan, *Acta Metall. Mater.*, **39**, No. 11: 2533 (1991).
27. R. Poduri and L.-Q. Chen, *Acta Mater.*, **46**, No. 11: 3915 (1998).
28. Y. Mishin, M. J. Mehl, and D. A. Papaconstantopoulos, *Acta Mater.*, **53**, No. 15: 4029 (2005).
29. W. B. Pearson, *Handbook of Lattice Spacing and Structure of Metals and Alloys* (New York: Pergamon Press: 1958), vol. **1**; W. B. Pearson, *Handbook of Lattice Spacing and Structure of Metals and Alloys* (New York: Pergamon Press: 1968), vol. **2**.
30. V. Vaithyanathan, *Phase-Field Simulations of Coherent Precipitate Morphologies and Coarsening Kinetics* (Ph.D. Thesis in Material Science and Engineering) (Pennsylvania State University, USA: 2002).
31. I. M. Lifshitz and V. V. Slyozov, *J. Phys. Chem. Sol.*, **19**, Nos. 1–2: 35 (1961).
32. C. Wagner, *Z. Electrochem.*, **65**, No. 7: 581 (1961).
33. A. J. Ardell, *Acta Metall.*, **20**, No. 1: 61 (1972).
34. D. G. Chellman and A. J. Ardell, *Acta Metall.*, **22**, No. 5: 577 (1974).
35. C. K. L. Davies, P. Nash, and R. N. Stevens, *Acta Metall.*, **28**, No.2: 179 (1980).
36. R. Toral, A. Chakrabarti, and J. D. Gunton, *Phys. Rev. B*, **39**, No. 1: 901 (1989).
37. A. Chakrabarti, R. Toral, and J. D. Gunton, *Phys. Rev. B*, **39**, No. 7: 4386 (1989).